



## Reconstructing warm-season temperatures using brGDGTs and assessing biases in Holocene temperature records in northern Fennoscandia

Gerard A. Otiniano<sup>a,\*</sup>, Trevor J. Porter<sup>a</sup>, Michael A. Phillips<sup>b</sup>, Sari Juutinen<sup>c</sup>, Jan B. Weckström<sup>d,e</sup>, Maija P. Heikkilä<sup>d,e</sup>

<sup>a</sup> Department of Geography, Geomatics and Environment, University of Toronto - Mississauga, 3359 Mississauga Rd, Mississauga, Ontario L5L 1C6, Canada

<sup>b</sup> Department of Biology, University of Toronto - Mississauga, Mississauga, Ontario, Canada

<sup>c</sup> Finnish Meteorological Institute, Climate System Research, Helsinki, Finland

<sup>d</sup> Environmental Change Research Unit, Ecosystems and Environment Research Programme, Faculty of Biological and Environmental Sciences, University of Helsinki, Finland

<sup>e</sup> Helsinki Institute of Sustainability Science, University of Helsinki, Finland



### ARTICLE INFO

Handling Editor: Dr. P. Rioual

**Keywords:**

Holocene  
brGDGT  
Fennoscandia  
Paleoclimate  
Biomarker

### ABSTRACT

Understanding Holocene climate variability is crucial for predicting future climate change, which will disproportionately affect high-latitude regions. Summer temperature ( $T_{\text{summer}}$ ) reconstructions in regions such as northern Finland are mainly derived from microfossil data. We reconstructed  $T_{\text{summer}}$  spanning the interval 10–1 cal ka BP using branched glycerol dialkyl glycerol tetraethers (brGDGTs) from lake-sediment record from Lake Annan Juomusjärvi (AJU) in northern Finland. The reconstruction shows cool early Holocene conditions,  $\sim 2^{\circ}\text{C}$  below the long-term mean (defined by the last 8.5 kyr), followed by persistent warming to a thermal maximum around  $\sim 7.0$  cal ka BP, a relatively stable climate ( $\sim 0.5^{\circ}\text{C}$  above the long-term mean) from 7.0 to 3.5 cal ka BP, and then a long-term cooling trend ( $-0.1^{\circ}\text{C}\cdot\text{kyr}^{-1}$ ) since 3.5 cal ka BP. This temperature history is remarkably well replicated by the nearby pollen- $T_{\text{July}}$  reconstruction from Lake Loitsana. However, Lake Loitsana chironomid and macrofossil data argue for a much earlier thermal maximum at  $\sim 10$  cal ka BP. Comparison of chironomid versus pollen records from across northern Fennoscandia confirms this inter-proxy discrepancy on the timing of Holocene peak warmth is a regional-scale phenomenon. Previous studies had raised the possibility that non-climatic noise in certain pollen records, due to local-scale overrepresentation of certain pollen types in the early and mid Holocene, may be contributing to an artificial lag in the thermal maximum. However, brGDGTs are unaffected by terrestrial flora and corroborate a mid-Holocene thermal maximum, which challenges the notion that pollen records are generally prone to misrepresenting the early to mid-Holocene climate history. Alternatively, proxy-specific environmental or mean seasonality biases may explain inter-proxy discrepancies in the timing of peak warmth. Continued diversification of the proxy network will help to better understand inter-proxy differences and refine knowledge of Holocene climate in northern Fennoscandia.

### 1. Introduction

The Holocene epoch, spanning the last 11,700 years, offers insight into natural climate variation during the present interglacial and serves for contextualizing the impact of anthropogenic activity on the climate system. Recent warming in the Arctic, up to 4 times greater than the global average (Rantanen et al., 2022), is significant in a historical context and there is growing consensus that, in some areas, this warming is becoming increasingly important in the context of the Holocene (Kaniewski et al., 2020; Marcott et al., 2013; Marsicek et al., 2018;

Porter et al., 2019; Ruddiman et al., 2016). The compounding of positive feedbacks (e.g., surface albedo changes due to a greening tundra and northward migrating treeline; (Webb et al., 2021) is thought to amplify warming in high-latitude regions (England et al., 2021; Previdi et al., 2021; Serreze and Barry, 2011). Moreover, the magnitude of warming is spatially heterogeneous due in large part to coupled climate and sea-ice processes, with greater potential for amplified warming in areas of northern Russia and northern Fennoscandia that are proximal to northern seas (e.g., Huang et al., 2017; Previdi et al., 2021). Such areas require special attention to better understand high-latitude climate

\* Corresponding author.

E-mail address: [gerard.otiniano@mail.utoronto.ca](mailto:gerard.otiniano@mail.utoronto.ca) (G.A. Otiniano).

dynamics and forecast what future environments may look like.

Northern Fennoscandia offers an attractive opportunity for studying Holocene climate conditions given the high abundance of freshwater lakes containing sediments that date to the early Holocene (Kaufman et al., 2020). Lake sediment cores from this region have been used to develop over 30 independent temperature reconstructions spanning the last 9–11 kyr (Fig. 1). These reconstructions derive from three main proxy types including: pollen ( $n = 16$ ), chironomids ( $n = 11$ ), and diatoms ( $n = 4$ ; Fig. 1; Kaufman et al., 2020). The presence of aquatic and wetland plant macrofossils from lake-sediment records in Fennoscandia ( $n = 5$ , not shown) have also been used as an indicator of early Holocene temperatures (11.7–7.5 cal ka BP; Shala et al., 2017; Välimäki et al., 2015). At the global scale, these same proxy records have been used to constrain the global mean annual temperature (e.g., Kaufman et al., 2020; Kaufman and Broadman, 2023), but in northern Fennoscandia they are interpreted as July temperature proxies (e.g., Autio and Hicks, 2004; Bigler and Hall, 2003; Larocque and Hall, 2004; Välimäki et al., 2015). Despite this presumed mid-summer seasonality alignment, the timing of the peak Holocene warmth in many pollen-based temperature reconstructions in Fennoscandia occurs in the mid Holocene around ~6–7 cal ka BP, which is ~3 kyr after peak Holocene temperatures observed in the majority of chironomid- and macrofossil-based reconstructions in this region (e.g., Shala et al., 2017; Välimäki et al., 2015). A closer agreement between peak June insolation and the chironomid- and macro-fossil-based  $T_{July}$  estimates is one line of evidence that has been used to argue for an early Holocene thermal maximum in this region (e.g., Shala et al., 2017). The apparent failure of pollen-based temperature reconstructions to capture early Holocene peak warmth has been attributed to local (catchment-scale) noise caused by the overrepresentation of certain pollen types (e.g., Välimäki et al., 2015). However, alternative explanations such as proxy-specific seasonality differences remain unexplored. The application of independent paleothermometers is needed to further our knowledge of Fennoscandia's Holocene temperature history and help to resolve the potential causes of inter-proxy disparities.

We reconstruct temperatures spanning most of the Holocene from ~10 to 1 cal ka BP using a regionally novel summer temperature proxy, branched glycerol dialkyl glycerol tetraethers (brGDGTs), from a lake-sediment core in northern Finland. This is the first application of this proxy to Holocene climate reconstruction in northern Fennoscandia.

BrGDGTs are membrane lipids synthesized by bacteria (Chen et al., 2022; Halamka et al., 2022; Sinninghe Damsté et al., 2011, 2018; Weijers et al., 2006) in a wide variety of terrestrial and aquatic environments (e.g., peats, soils, lakes, and rivers; Raberg et al., 2022a,b). The relative abundance of the varied brGDGT types (see Sect. 2.2) is influenced by environmental conditions such as water chemistry and in-situ temperature, which enables estimation of past climate and environmental variables from fossil assemblages of brGDGTs preserved in the geological record (e.g., De Jonge et al., 2014; Otiniano et al., 2023; Raberg et al., 2021; Weijers et al., 2007; Zhao et al., 2021). In high-latitude regions, the temperature sensitivity of lacustrine brGDGTs is biased to average warm-season conditions, quantified by the mean of monthly temperatures above freezing (MAF; Martínez-Sosa et al., 2021; Naafs et al., 2017; Otiniano et al., 2023; Raberg et al., 2021), and therefore provides an opportunity to reconstruct MAF variability in Fennoscandia through the Holocene. This proxy has a broader seasonal response compared to what has been assumed for the other major  $T_{July}$  temperature proxies from this region – pollen, chironomids, diatoms, and macrofossils – and, therefore, provides a novel perspective on the warm-season paleoclimate history of Fennoscandia.

## 2. Methods

Our study lake is Lake Annan Juomasjärvi (AJU, 69.254°N, 27.406°E, 195 m above sea level) in the Lake Jänkäjärvi catchment area in the municipality of Inari, northern Finland (Fig. 1). The lake AJU surface area is 0.066 km<sup>2</sup>, has a maximum depth of 6 m, and is likely groundwater fed through an esker along the western margin of the lake and surface fed through multiple channels. The lake faces an esker system in the west, and its catchment is covered by pine (*Pinus sylvestris*) and downy birch (*Betula pubescens* ssp. *czerepanovii*) forests on sandy soils. The nearest climate station is Inari Väylä, approximately 20 km East of the study area. The mean annual temperature (MAT) of observations from 1991 to 2020 CE is −0.5 °C. From May to September, monthly average temperatures remain above 0 °C, with a MAF of 9.1 °C. Precipitation amounts are not available from the Inari Väylä climate station, but precipitation amounts from the climate station Inari Kaamanen, 10 km Southwest of lake AJU, indicate a mean annual precipitation amount of 459 mm.

A 1.25-m long sediment core was collected from lake AJU in March

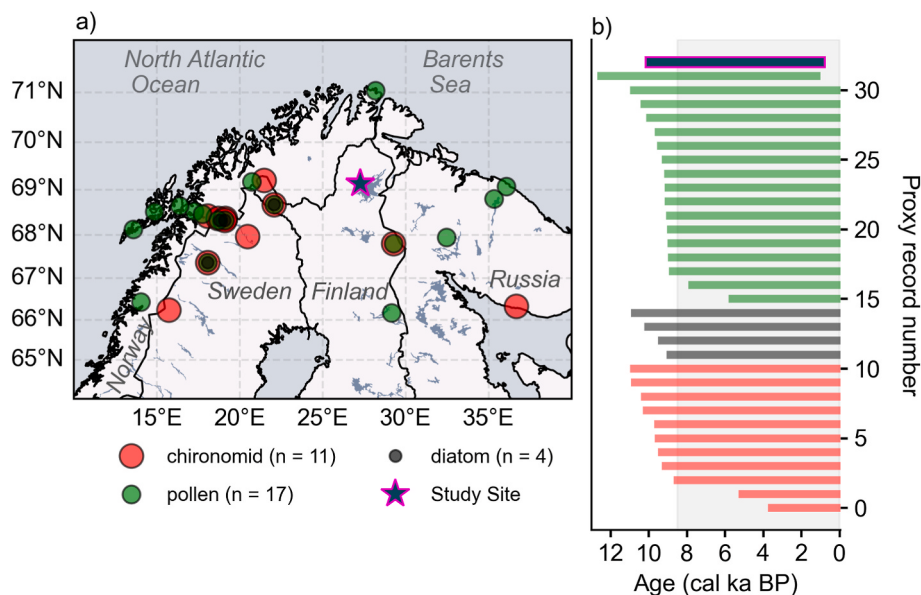


**Fig. 1.** (a) Map of local Utsjoki Kevo climate station and lake AJU (star) as well as other Fennoscandian paleotemperature reconstructions based on pollen, chironomids, and diatoms. (b) Temporal coverage of each paleorecord plotted in the map; grey-shaded area illustrates the 8.2 cal ka BP-present period that is common to most of the paleorecords and used as a baseline for standardising the reconstructions for comparative purposes.

2017 using a Livingstone-type piston corer (core diameter 4.5 cm). Adjacent to the piston core, a surface core preserving the loose sediment layers at the sediment-water interface was taken using a HTH Kajak gravity corer (Renberg and Hansson, 2008). In addition, surface soils ( $n = 19$ ) from the catchment area, benthic algal mats from lake AJU ( $n = 1$ ) and from a second nearby lake ( $n = 4$ ) were collected during the growing season in August 2018. The long piston sediment core was subsampled at 1-cm resolution, which yielded 125 samples. A Holocene GDGT record was developed exclusively from the Livingstone core materials from core depths greater than 15 cm only. The lake and soil sediment samples were freeze-dried, and then processed for lipid extraction.

An age model for the lake AJU core was developed using a modern age (2017 CE, year of sampling) for the surface and AMS radiocarbon dates from 10 plant macrofossils and 3 bulk sediment samples from the long core (SI, Fig. S1). Radiocarbon measurements were performed at Poznań Radiocarbon Laboratory (SI). The chronology was constrained in Bayesian age-depth modelling in rbacon (v. 2.5.8; Blaauw and Christen, 2011) using the IntCal20 calibration curve (Reimer et al., 2020) and default parameters (segment length of 5 cm, accumulation shape of 1.5, and accumulation rate of 20). The surface core was dated by  $^{210}\text{Pb}$  and  $^{137}\text{Cs}$  at the Liverpool University Environmental Radioactivity Laboratory. A rapid change in concentration of unsupported  $^{210}\text{Pb}$  at ca. 17-cm depth in the record was observed (Fig. S2), suggesting a significantly lower sedimentation rate below this layer, in agreement with the  $^{14}\text{C}$ -constrained age-depth profile of the long core. However, the abrupt change in the supported  $^{210}\text{Pb}$  concentrations at 17 cm in the surface core may also indicate a hiatus in the sediment record. Due to a lack of any clear visual sedimentological tie-point between the surface and long cores, we thus do not include the surface-core  $^{210}\text{Pb}$  and  $^{137}\text{Cs}$  age estimates in the long-core age-model. Due to the general lack of high-precision age-constraints from the uppermost sediments, chronological uncertainty tends to be greater in the late Holocene after  $\sim 2$  cal ka BP. Regardless, our analysis of the GDGT record focuses on long-term, millennial scale trends, which can be adequately characterised given uncertainties in the age model.

Approximately 4 g of freeze-dried lake-sediment from each 1 cm-increment were used for lipid analysis. Collection of the total lipid extract, purification of the compound of interest, and brGDGT quantification followed procedures outlined in Otiniano et al. (2023, 2020). Raw data analysis and peak integration was performed in Analyst 1.7.2. (Sciex).

GDGT data were analysed in the Python environment (3.10.5) with the Pandas (1.4.4; McKinney, 2010; Reback et al., 2022), Numpy (1.23.2; Harris et al., 2020), Pyleoclim (0.9.1; Khider et al., 2022), and Cartopy (0.21.0; Elson et al., 2022) packages.

## 2.1. Inferring environmental conditions from brGDGT distributions

The structures of brGDGTs are variable, containing up to 2 cyclopentane moieties and 4–6 methyl groups (Sinninghe Damsté et al., 2000). Moreover, the penta- and hexamethylated brGDGTs contain multiple isomers that are differentiated by the positions of methyl groups (5-methyl, 6-methyl; De Jonge et al., 2013). The temperature sensitivity of brGDGT distributions is typically expressed as the degree of methylation of branched tetraethers (MBT<sub>5Me</sub>; Eq. (1); De Jonge et al., 2014; Martínez-Sosa et al., 2021; Russell et al., 2018; Weijers et al., 2007).

$$\text{MBT}_{5\text{Me}}' = \frac{\text{Ia} + \text{Ib} + \text{Ic}}{\text{Ia} + \text{Ib} + \text{Ic} + \text{IIa} + \text{IIb} + \text{IIc} + \text{IIIa}} \quad (1)$$

Alternative methods of determining temperatures from brGDGT distributions include the multilinear regressions of brGDGT fractional abundances (e.g., Parish et al., 2023; Raberg et al., 2022b, 2021) and, in high-latitude lakes, the fractional abundance of the IIIa brGDGT (IIIa<sub>fa</sub>; Otiniano et al., 2023).

In mid- and high-latitude lakes, brGDGTs typically display a warm-

season sensitivity, which is likely driven by enhanced biological activity during the warm-season (e.g., Martínez-Sosa et al., 2021; Otiniano et al., 2023; Raberg et al., 2021) and the decoupling of lake water and air temperature as a result of the insulating effect of lake ice (Cao et al., 2020). This bias is evidenced by observations of higher lacustrine brGDGT concentrations during summer months in mid- and high-latitude lakes (e.g., Qian et al., 2019; Zhao et al., 2021). The temperature and environmental sensitivities of brGDGTs varies with depositional environment (Dang et al., 2018; Otiniano et al., 2023) and environmental conditions that likely influence bacterial community composition (e.g., Bechtel et al., 2010; De Jonge et al., 2019; van Bree et al., 2020). The reliability of temperature estimates from brGDGT distributions is therefore dependent on environmentally appropriate calibrations of brGDGT distributions to climate conditions. In soils, the reliability of brGDGT-derived temperature estimates can also be inferred from the isomerization ratio (IR; Eq. (2); De Jonge et al., 2015), which quantifies the proportion of temperature sensitive 5-methyl brGDGTs to the comparatively temperature insensitive 6-methyl brGDGTs. Similarly, the isomerization of branched tetraethers (IBT; Eq. (3); Ding et al., 2015) also provides insight into the ratio of uncyclized 6- to 5-methyl brGDGTs.

$$\text{IR} = \frac{\text{IIa}' + \text{IIb}' + \text{IIc}' + \text{IIIa}' + \text{IIIb}' + \text{IIIc}'}{\text{IIa} + \text{IIa}' + \text{IIb} + \text{IIb}' + \text{IIc} + \text{IIc}' + \text{IIIa} + \text{IIIa}' + \text{IIIb} + \text{IIIb}' + \text{IIIc} + \text{IIIc}'} \quad (2)$$

$$\text{IBT} = -\log \frac{\text{IIa}' + \text{IIIa}'}{\text{IIa} + \text{IIIa}} \quad (3)$$

Environmental conditions are inferred from indices such as the cyclization of branched tetraethers (CBT'; Eq. (4); De Jonge et al., 2014) and the degree of cyclization of brGDGTs (DC'; Eq. (5); Baxter et al., 2019; Sinninghe Damsté et al., 2009), which correlates well with pH and conductivity in lacustrine environments (Martínez-Sosa et al., 2020, 2021; Raberg et al., 2021). Further insight into environmental changes can also be illuminated by the ratio of branched to isoprenoidal tetraethers (BIT; Eq. (6); Hopmans et al., 2004), which has denoted changes in oxycline position (Baxter et al., 2021) as well as soil moisture content (Peaple et al., 2022).

$$\text{CBT}' = -\log \frac{\text{Ic} + \text{IIa}' + \text{IIb}' + \text{IIc}' + \text{IIIa}' + \text{IIIb}' + \text{IIIc}'}{\text{Ia} + \text{IIa} + \text{IIIa}} \quad (4)$$

$$\text{DC}' = \frac{\text{Ib} + \text{IIb} + \text{IIb}'}{\text{Ia} + \text{IIa} + \text{IIa}' + \text{Ib} + \text{IIb} + \text{IIb}'} \quad (5)$$

$$\text{BIT} = \frac{\text{Ia} + \text{IIa} + \text{IIa}' + \text{IIIa} + \text{IIIa}'}{\text{Ia} + \text{IIa} + \text{IIa}' + \text{IIIa} + \text{IIIa}' + \text{crenarchaeol}} \quad (6)$$

The applicability of brGDGT paleothermometry in this region is supported by their application in proximal regions like Iceland (e.g., Harning et al., 2020) and a previous global analysis of branched and isoprenoidal GDGTs ( $n = 90$ ), which included lacustrine GDGT samples from Finland ( $n = 29$ ; Pearson et al., 2011). The analysis inferred a strong temperature dependence of the antiquated MBT index, which does not distinguish between 5-methyl and 6-methyl brGDGT isomers (Pearson et al., 2011). However, recent studies demonstrate the importance of separating the 5-methyl and 6-methyl brGDGT isomers for paleoclimate applications (De Jonge et al., 2013), which has only been made practical with recent chromatographic technological advancements (Hopmans et al., 2016).

In this study, temperatures are estimated from the lake AJU brGDGT record by developing novel high-latitude specific brGDGT-temperature transfer functions. While agglomerative nesting analysis suggests that the temperature sensitivity of high-latitude lacustrine brGDGTs is shared by some mid-latitude lake brGDGTs (O'Beirne et al., 2023), it is important to consider that this temperature sensitivity demonstrates latitude-based variations (Zhao et al., 2023). Moreover, the temperature

sensitivity of high-latitude lacustrine brGDGTs can vary at regional and subregional scales (Otiniano et al., 2023) and may be influenced by constraints on growing-season conditions such as lake-ice duration (e.g., Cao et al., 2020), which is dependent on latitude. As such, environmentally appropriate calibration datasets are paramount to applications of brGDGT paleothermometry. In the absence of modern lacustrine brGDGTs in Fennoscandia, we develop brGDGT-temperature transfer functions using a network of 117 high-latitude ( $>55^{\circ}\text{N}$ ) modern lacustrine samples spanning 57.2 to 72.6 °N and 14.6 to 161.1 °W (e.g., Martínez-Sosa et al., 2021; Otiniano et al., 2023; Raberg et al., 2021; Zhao et al., 2021) for inferring the local Holocene temperature history.

ERA5 2-m air temperature reanalysis data ( $0.25^{\circ} \times 0.25^{\circ}$  spatial resolution; Hersbach et al., 2020) were used to define MAF values for each site. Transfer functions relating MBT<sup>5Me</sup> and IIIa indices to MAF were calibrated to via ordinary least-squares (OLS) regression. Additionally, a step-backward regression analysis was used to develop a multilinear model for MAF estimation that includes all brGDGT fractions that are significantly ( $p < 0.01$ ) correlated with MAF, as outlined by Raberg et al. (2021) and Parish et al. (2023). Given the limited sample size for developing a high-latitude brGDGT-temperature regression model, the Root Mean Squared Error (RMSE) terms are calculated using K-Fold Cross-Validation with 3, 5 and 10 folds (O'Beirne et al., 2023; Pérez-Angel et al., 2020).

## 2.2. Proxy record compilations

Comparing the records reported here to previously published Holocene climate reconstructions is complicated by the irregular and unequal sampling frequency of independently reconstructed records, which impede the application of typical tests of correlation. Although sample size and frequency can be artificially equated via interpolation, such methods bias power spectra, thus further complicating efforts to assess synchronicity between records (e.g., Rehfeld et al., 2011). In this study, independent records of Holocene climate reported in the Temperature-12 K dataset (SI; Kaufman et al., 2020) and in Shala et al. (2017) were compiled by proxy type (pollen, diatoms, and chironomids) and binned by averaging the records into 400-year intervals to produce three mean records of Holocene climate in northern Fennoscandia. Before binning, temperature anomalies were calculated for each record relative to the mean temperature for the period 8.5 cal ka BP to present, a common period for all but five of the thirty-one available records (Fig. 1). The anomaly temperatures of one pollen record that spans 2.0–12.0 cal ka BP are reported relative to the mean temperature from 2.0 to 8.5 cal ka BP, while other chironomid and pollen records that fall short of 8.5 kyr are each reported relative to the mean of the full record. The proxy records discussed here are also compared to monthly insolation curves (Laskar et al., 2004) expressed relative to present day.

## 2.3. brGDGT provenance

The source of brGDGTs in lake AJU from either in situ production or from contributions of terrestrial organic matter (i.e., soils), must be established before environmental or climatic conditions are reconstructed (e.g., Naeher et al., 2014) as the environmental sensitivity of brGDGTs varies with depositional environment (e.g., Dang et al., 2018; Otiniano et al., 2023). Identifying brGDGT provenance is challenging as different environments can produce similar distributions. Although there is no universal method of differentiating brGDGT sources, past studies have developed site-specific environment-discriminating methods that rely on the observed differences in GDGT proportions between depositional settings (e.g., Dang et al., 2018; De Jonge et al., 2015; Martin et al., 2019; Sinninghe Damsté et al., 2009; Zell et al., 2014) and comparisons of intact polar lipids (Raberg et al., 2022a). In addition, machine-learning methods have recently been applied to help provenance GDGT assemblages but may not yet be well trained for high-latitude environments (e.g., due to low sample numbers) given that

brGDGTs from the Lake AJU records are classified as *marine* using the BIGMaC algorithm (Martínez-Sosa et al., 2023). Here, the source of brGDGTs in lake AJU is explored via comparison of the DC', MBT<sup>5Me</sup>, IR, IBT, CBT', and BIT indices of modern soil, lake sediment, and core-top samples.

## 3. Results and discussion

### 3.1. Biomarker sources and sensitivity

Differences between modern terrestrial and lacustrine GDGT assemblages in this region of the Finnish Lapland are observed by comparing GDGT abundances and indices of modern soil samples to lacustrine samples, (i.e., algal mats (benthic biofilms) and sediments). The brGDGT distributions from soils, algal mats, and core-top sediments (15–20 cm) from lake AJU are dominated by Ia, IIa, IIIa (Figs. 2 and SI). However, the relative abundance of brGDGTs Ia, IIa, and IIIa are more similar to the algal mat and core-top samples than the soils (Fig. S3), suggesting a limnological provenance of brGDGTs that are preserved in the lake AJU sediment record.

Significant differences are observed between brGDGT distributions from soils and biofilms with respect to the IR ( $t = 7.06$ ,  $p < 0.001$ ) index (Fig. 3). Opportunely, the IR index has been previously employed to differentiate soil and lacustrine brGDGT-producing environments in China (Dang et al., 2018). Meanwhile, conjunctive application of the DC' and MBT<sup>5Me</sup> indices (prior to the differentiation of 5- and 6-methyl brGDGTs) have previously been used to differentiate between brGDGT sources (Sinninghe Damsté et al., 2009; Zell et al., 2014). Applying this approach to soil and biofilm DC' and MBT<sup>5Me</sup> values from the lake AJU region displays unique clustering of the two groups. Predominant in situ production is inferred from the DC'-MBT<sup>5Me</sup> values of lake AJU as the upper (i.e. younger) half of the sediment core more closely overlaps with lake AJU benthic biofilm values and the lower (i.e. older) half of the sediment core coincides with values observed in other high-latitude lakes (e.g., Otiniano et al., 2023, Fig. 4). However, it is important to note that the distribution of brGDGTs from modern Fennoscandian lakes in the DC'-MBT<sup>5Me</sup> space is unknown and future efforts to characterize lacustrine brGDGTs from this region are needed to verify the efficacy of comparing DC' and MBT<sup>5Me</sup> values to determine brGDGT provenance.

The DC'-MBT<sup>5Me</sup> values from lake AJU core sediments display a linear relationship with age (Fig. 4), which likely reflects climatic change rather than a change in brGDGT source. Cold conditions are associated with low MBT<sup>5Me</sup> values (e.g., Martínez-Sosa et al., 2021) and a low fractional abundance of Ia (e.g., Raberg et al., 2021), which would yield high DC' values (Eq. (5)). As such, a transition from colder to warmer conditions with time (Section 3.3) explains the linear trend observed in the DC' and MBT<sup>5Me</sup> space (Fig. 4).

Additionally, CBT' and IBT index values from the local soils and AJU benthic biofilm samples display significant differences (CBT'  $t = 3.80$ ,  $p < 0.01$ ; IBT  $t = 3.2109$ ,  $p < 0.01$ , Fig. 3). Both indices indicate the ratio of 6-methyl to 5-methyl brGDGT isomers and although the factor driving change in isomer proportions is unknown, differences of index values between local soil versus benthic biofilms again suggest lacustrine provenance of brGDGTs in the lake AJU record (Fig. 3).

The lake AJU GDGT record shows near-constant BIT values throughout the record, indicating little change in the proportion of brGDGTs and crenarchaeol (Fig. 2). The driver of variability in the BIT index is difficult to ascertain as these values are known to change with multiple factors including the oxycline position, precipitation, and GDGT provenance (e.g., Baxter et al., 2021; Peaple et al., 2022; Xu et al., 2020). As such, we interpret the long-term stability in the BIT index as an indication that lake AJU has remained geochemically and hydrologically stable throughout the Holocene.

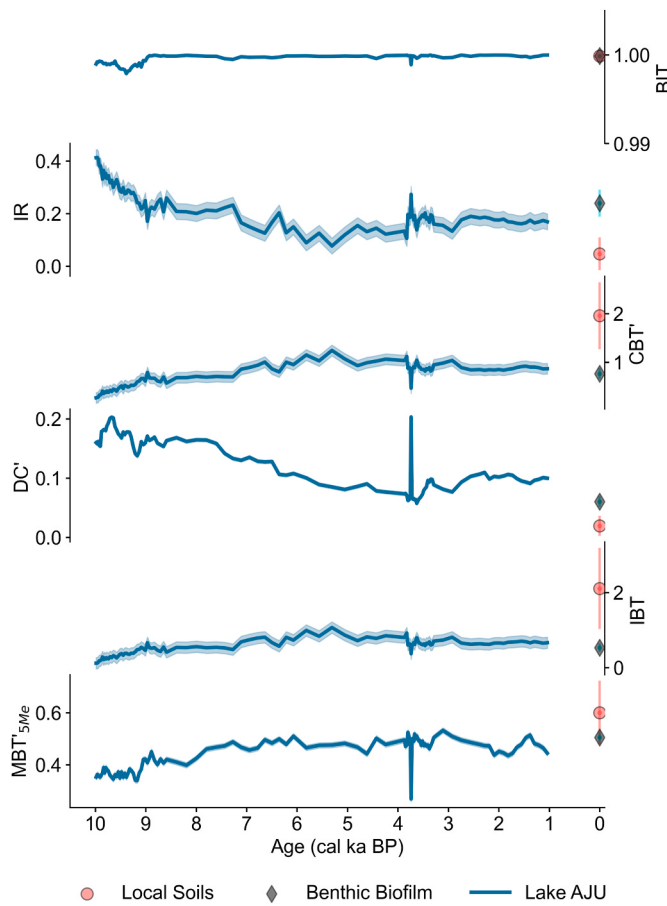


**Fig. 2.** BIT, IR, CBT', DC', IBT, and MBT'5Me index values (top to bottom) from local soils (red circle), benthic biofilms (blue diamond) and lake AJU (dark blue) with  $2\sigma$  uncertainty (shaded blue).

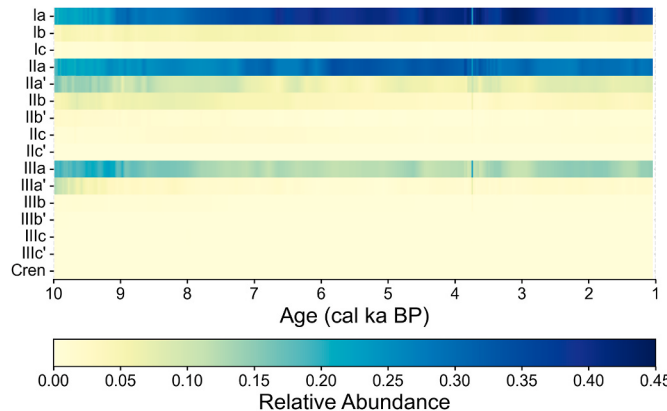


**Fig. 3.** Relative abundances of brGDGTs and Crenarcheol from lake AJU core record.

### 3.2. A brGDGT-MAF transfer function for high-latitude lakes

The compilation of brGDGT assemblages from lakes across high latitude regions (Fig. 5; Martínez-Sosa et al., 2021; Otiniano et al., 2023; Raberg et al., 2021; Zhao et al., 2021) display dominant temperature sensitivities of MBT'5Me and IIIa<sub>fa</sub> to MAF. OLS calibration of the MBT'5Me index to MAF from this high-latitude site network (Eq. (7)) explains a higher degree of variability (adj R<sup>2</sup> = 0.65, RMSE = 1.2 °C, n = 117; Fig. 5) compared to other recent calibration studies of lacustrine

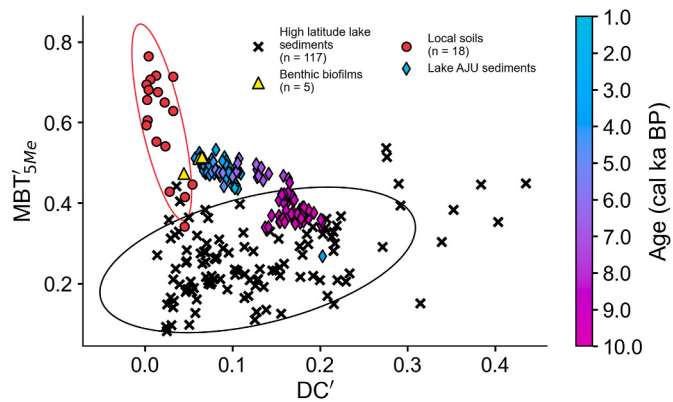


**Fig. 4.** Scatterplot of DC' and MBT'5Me values from lake AJU benthic biofilms (diamonds, colour-coded according to age), local soils (red circles), lake AJU sediment core samples (yellow circles), and modern lake sediments from a circumpolar network of high-latitude lacustrine sites.

brGDGTs from a smaller network of high-latitude North American sites (adj R<sup>2</sup> = 0.53, RMSE = 1.0 °C, n = 67; Otiniano et al., 2023) and it outperforms the recent global Bayesian lake calibration (adj R<sup>2</sup> = 0.42, RMSE = 2.9 °C, n = 272; Martínez-Sosa et al., 2021).

$$MAF(\text{°C}) = 18.8 \times MBT'_{5Me} + 2.1 \quad (7)$$

Similarly, IIIa<sub>fa</sub> from this expanded high-latitude dataset (Eq. (8)) explains more variation in MAF (adj R<sup>2</sup> = 0.64, RMSE = 1.2 °C, n = 117; Fig. 5) than the high-latitude North American network alone (R<sup>2</sup> = 0.60, RMSE = 1.1 °C, n = 67).

$$MAF(\text{°C}) = -14.0 \times IIIa_{fa} + 11.0 \quad (8)$$

Finally, a multilinear regression analysis of brGDGT fractional abundances against MAF indicates significant relationships ( $p < 0.01$ ) for IIa<sub>fa</sub>, IIIa<sub>fa</sub>, IIa'<sub>fa</sub>, and IIIb<sub>fa</sub> (Eq. (9)). A multilinear backward-stepwise regression model that includes these fractions as MAF predictors (ML<sub>fa</sub>; Eq. (9); adj R<sup>2</sup> = 0.75, RMSE = 1.0 °C, n = 117; Fig. 5) outperforms all of the previously discussed brGDGT-MAF models from high-latitude North America and the global regression model, and a multilinear fractional abundance model by Raberg et al. (2021) that includes lacustrine brGDGTs from eastern high-latitude Canada, Iceland, Central Europe, East Africa, and China (adj R<sup>2</sup> = 0.43, RMSE = 2.0 °C, n = 182). The higher accuracy observed in the high-latitude lacustrine brGDGT-temperature transfer function, in contrast to the global regression model, can be attributed to the relatively narrow range of environmental conditions and temperature fluctuations characteristic of the high-latitude environment. This unique transfer function suggests that brGDGT temperature sensitivity varies regionally. Although the lower accuracy of the western high latitude North American transfer function seemingly contradicts this finding, this discrepancy can likely be explained by the higher variability surrounding a narrower range of temperatures in the North American calibration dataset, as well as the smaller sample size used in that region. Further research investigating regional lacustrine brGDGT temperature sensitivity is essential to better understand these variations and provide more comprehensive insights.

$$MAF(\text{°C}) = 17.0 - 11.4 \times IIa_{fa} - 17.4 \times IIIa_{fa} - 15.9 \times IIa'_{fa} - 124.4 \times IIIb_{fa} \quad (9)$$

For the purpose of paleoclimate estimates from the AJU brGDGT record, we apply the ML<sub>fa</sub> calibration (Eq. (9)) owing to its superior performance (adj. R<sup>2</sup> = 0.75) across a vast network of high-latitude sites and lowest prediction error (RMSE = 1.0 °C) among the three different models. Although the absence of the top 15 cm of the Lake AJU sediment core bars a direct comparison of actual and estimated MAF values from the brGDGT record, estimated MAF values from a benthic biofilm in

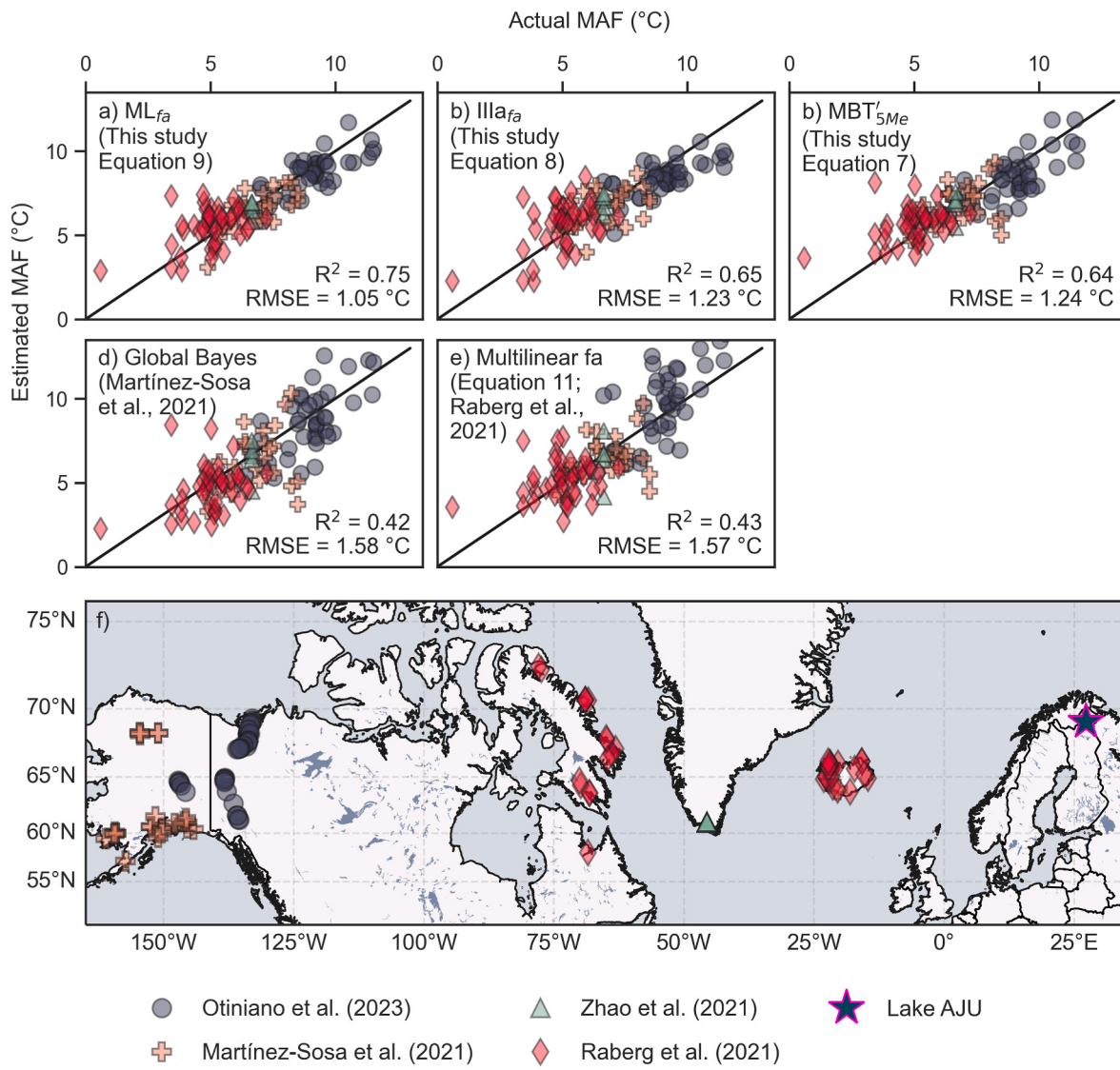


**Fig. 5.** (a) Scatterplots of actual versus estimated MAF based on different regression models:  $ML_{fa}$  (this study - Eq. (9)), (b)  $IIIa_{fa}$  (this study - Eq. (8)), (c)  $MBT'_{5Me}$  (this study - Eq. (7)), (d) global multilinear fractional abundance (Equation 11; Raberg et al., 2021) and (e) global Bayesian calibration (Martínez-Sosa et al., 2021). (f) Map of high latitude lacustrine sites included in temperature calibrations (A)–(C) are included (Martínez-Sosa et al., 2021; Otiniano et al., 2023; Raberg et al., 2021; Zhao et al., 2021).

Lake AJU ( $9.4 \pm 1.0$  °C) closely aligns with modern (1990–2021 CE) MAF values (9.1 °C, Fig. S1), supporting the application of the  $ML_{fa}$  model in this region.

It is important to note that mean monthly temperatures undoubtedly changed during the Holocene. As a result, the range of months incorporated into the MAF variable likely changed between warmer and colder periods of the Holocene. For example, brGDGT production during colder months (April and October) may have slowed during colder periods like the early Holocene. However, the influence of this change is likely low as lacustrine brGDGT production persists in regions that experience winter temperatures below freezing (Cao et al., 2020; Zhao et al., 2021). Moreover, normalizing the brGDGT-derived MAF estimates over the last 8.5 kyr yields a relative record of MAF change, which also permits inter-proxy comparisons of climate records. Future studies that seek to characterize the seasonal production of brGDGTs in this region will improve understanding of how changes in monthly temperatures could influence brGDGT-derived climate reconstructions during relatively cold and warm periods in Fennoscandia.

### 3.3. brGDGT-based temperature reconstruction

The brGDGT-derived MAF reconstruction from lake AJU spans ~10.0 to 1.0 cal ka BP, making it one of the few temperature reconstructions in Fennoscandia to reach 10 cal ka BP (Figs. 1 and 2). The MAF reconstruction indicates temperature anomalies of ~−1.8 °C between 10.0 and 9.9 cal ka BP (Fig. 6a). Cool early Holocene conditions coincide with the recession of the Scandinavian Ice Sheet towards the Scandinavian mountain range; however, the ice sheet persisted as a prominent landscape feature until approximately 9.7 cal ka BP (Stroeven et al., 2016), likely exerting a continued depressive influence on the regional energy balance. The presence of the ice sheet likely decreased the regional surface energy such that northern sites in closer proximity to the ice sheet would have experienced a more pronounced cooling effect compared to more southern sites.

From 9.5 to 6.0 cal ka BP, the MAF reconstruction indicates warming into the mid-Holocene at a rate of ~0.8 °C kyr<sup>−1</sup>. This warming trend aligns closely in both timing and rate with a pollen-derived temperature reconstruction from Lake Loitsana, located 107 km southeast of Lake AJU (Fig. 6a; Shala et al., 2017). In many records in continental

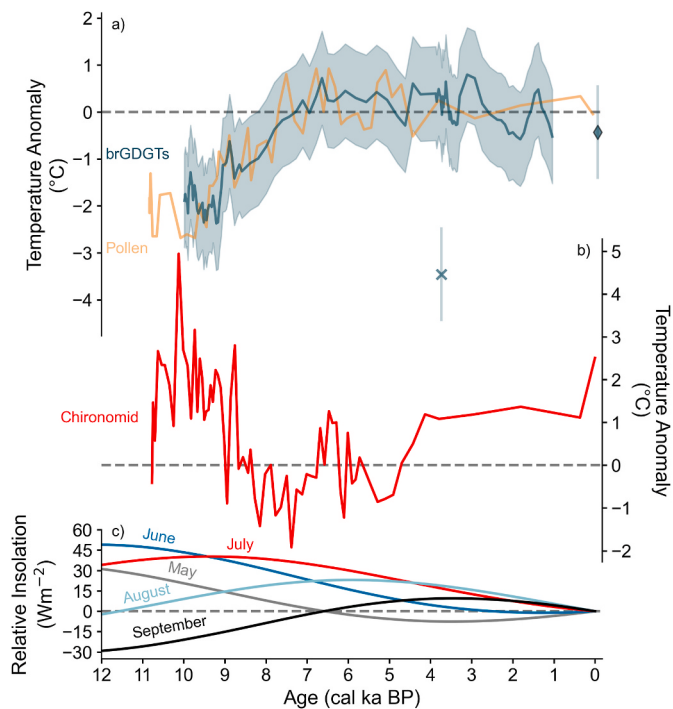


**Fig. 6.** (a) Reconstructed MAF relative to modern from the brGDGT record of Lake AJU (blue) using the  $ML_{fa}$  transfer function (Eq. (9)); individual markers are used to highlight an outlier datapoint at 3.7 cal ka BP (blue x) and a modern MAF estimate based on the benthic biofilm (blue diamond); a pollen-derived temperature reconstruction from Lake Loitsana is also plotted (orange; Shala et al., 2017). (b) Chironomid-derived temperatures from Lake Loitsana (red; Shala et al., 2017). (c) Relative monthly insolation trends through the Holocene at 65°N (Laskar et al., 2004) are plotted for May (grey) June (dark blue), July (red), August (light blue), and September (black) (b).

Northern Europe, Holocene peak warmth is delayed by millennia from the June insolation maximum (Sejrup et al., 2016; Seppä et al., 2009 and references within). The delay has been attributed to the albedo and meltwater effects of the decaying Laurentide Ice Sheet, further influencing the strength of the Atlantic overturning circulation and downstream climate (Cartapanis et al., 2022; Renssen et al., 2012). However, a delayed thermal maximum coinciding with mid-Holocene could be attributed to several other factors, including the influence of late-summer insolation trends (Fig. 6c), positive feedbacks such as reduced surface albedo driven by a northward migrating treeline into the deglaciated terrain (e.g., Foley et al., 1994), and the influence of relatively warm Atlantic waters into the Barents Sea (Andersen et al., 2004; Duplessy et al., 2005). These warmer Atlantic waters were associated with a strengthened Norwegian Current from approximately 10.0 to 6.5 cal ka BP (Sjögren, 2021 and references within).

The brGDGT-based MAF reconstruction also shows that the 10.0 to 6.5 cal ka BP warming trend was punctuated by sub-millennial-scale variability. Compared to the start of the reconstruction, cooler temperatures are reconstructed from 9.7 to 9.2 cal ka BP, with a mean temperature anomaly of around  $-2.1^{\circ}\text{C}$  defining the latter half of this period (Fig. 6a). Subsequently, reconstructed temperatures show a rapid increase, warming nearly  $\sim 2^{\circ}\text{C}$  from 9.2 to 8.9 cal ka BP (Fig. 6a). The Loitsana pollen-temperature reconstruction shows a warming trend of a comparable magnitude from 9.7 to 8.9 cal ka BP (Fig. 6a). Both the AJU brGDGT- and Loitsana pollen-based reconstructions show a brief pause or reduction in warming rate from 8.9 to 8.2 cal ka BP, followed by a return to higher rates of warming from 8.2 to 6.5 cal ka BP (Fig. 6a). Both records show an overall temperature increase of  $\sim 2.8^{\circ}\text{C}$  from 9.5 to 6.5 cal ka BP (Fig. 6a).

At the regional scale, the periods of colder reconstructed conditions

or muted warming from 9.6 to 9.2 cal ka BP and 8.9 to 8.2 cal ka BP are corroborated by independent proxy records. The first cold event coincides with the so-called Erdalen Event 2 ( $\sim 9.7$  cal ka BP) which is captured in other pollen records from the Scandinavian Mountain range (Paus et al., 2006, 2019). Evidence for cooling between  $\sim 9.7$  and 9.2 cal ka BP is also inferred from geomorphic evidence for glacier advances in Norway (e.g., Aa and Sønstegaard, 2019; Dahl et al., 2002; Matthews and Dresser, 2008; Nesje, 2009; Nesje et al., 2006). Although cold conditions at 8.2 are recognized across the North Atlantic region as the 8.2 cal ka BP event, sustained cool conditions since 8.8 cal ka BP may be a unique feature to northern Fennoscandia during the early Holocene.

From 7.0 to 3.5 cal ka BP, brGDGT-reconstructed temperature anomalies were generally warmer than the long-term mean (Fig. 6a). During this interval, a peak temperature anomaly of  $+0.7^{\circ}\text{C}$  occurs by 6.7 cal ka BP (Fig. 6a). Similarly, the Lake Loitsana pollen record (Shala et al., 2017) indicates peak warmth at roughly the same time (Fig. 6a). This timing of peak warm-season conditions is closely aligned with the mean of July–September insolation trends (Fig. 6c), as may be expected for the brGDGT proxy which integrates the average warm-season conditions. For the remainder of the 7.0–3.5 cal ka BP period, reconstructed temperature anomalies varied from  $-0.3^{\circ}\text{C}$  to  $+0.7^{\circ}\text{C}$  but were mostly warmer than the long-term mean (mean anomaly =  $+0.3^{\circ}\text{C}$ ). However, there is one outlier datapoint at 3.7 cal ka BP that diverges from this pattern, showing an extremely cold temperature anomaly ( $-3.4^{\circ}\text{C}$ ; Fig. 6a), driven by a shift toward higher  $IIa_{fa}$ ,  $IIa'_{fa}$ ,  $IIIa'_{fa}$ , and  $IIb_{fa}$  and lower  $Ia_{fa}$  and  $IIa_{fa}$  relative abundance (Fig. 2). The changes in the brGDGT assemblage could be interpreted as a short-lived, high-magnitude cooling event. However, a cold event of this magnitude is not observed in any of the other temperature reconstructions from Fennoscandia and there is no clear driver of climatic cooling at this time. Instead, this change in brGDGT distribution may indicate possible limnological changes. For example,  $IIa_{fa}$ ,  $IIa'_{fa}$ ,  $IIIa_{fa}$ , and  $IIIa'_{fa}$  significantly vary with conductivity and pH and the simultaneous reduction of  $IIa_{fa}$  and increase of  $IIb$ ,  $IIIa$ , and  $IIIa'$  is consistent with a possible increase in alkalinity (e.g., Raberg et al., 2021). Alternatively, an increase in  $IIIa_{fa}$  is consistent with a decrease in dissolved oxygen and could therefore reflect anoxia at this time (e.g., Yao et al., 2020). However, in lieu of other proxy indicators to help understand the possible limnological origins we recommend that the temperature estimate associated with the 3.7 cal ka BP outlier should be interpreted with a high degree of caution.

After 3.5 cal ka BP, the Lake AJU temperature record indicates general cooling at an average rate of  $-0.1^{\circ}\text{C}\cdot\text{kyr}^{-1}$  (Fig. 6a). In Fennoscandia, widespread cooling over this interval is also interpreted from the increased lateral spread of peatlands (Korhola et al., 2010; Weckström et al., 2010) and also aligns with decreasing mean summer insolation (Fig. 6c). Late Holocene cooling is also observed more broadly in North Atlantic (Marsicek et al., 2018) and global temperature compilations (Kaufman et al., 2020). The general cooling trend in Lake AJU temperature reconstruction is also marked by considerable sub-millennial variability, similar in magnitude to what is observed in the mid-Holocene. For example, cooler reconstructed conditions after 2.8 cal ka BP are coincident with broad scale cooling in the North Atlantic, potentially related to Bond Event 2 (Wanner et al., 2011). However, we refrain from interpreting climatic signals after  $\sim 2.0$  cal ka BP given the large uncertainties in the Lake Annan Jänkäjärvi age model (Fig. S2, Section 2).

#### 3.4. Broader implications of the lake AJU temperature reconstruction

The Lake AJU brGDGT-temperature reconstruction corroborates the Lake Loitsana pollen-inferred Holocene temperature history (Shala et al., 2017) and suggests brGDGTs may have a broader role to play in

refining our understanding of Holocene climate change in northern Fennoscandia. Both reconstructions show a pronounced warming trend from the early- to mid-Holocene and a thermal maximum of comparable magnitude ( $\sim 0.5^{\circ}\text{C}$  above the long-term mean) at 6.7 cal ka BP. However, this result contrasts with other proxy-T<sub>July</sub> estimates from Lake Loitsana. For example, aquatic plant macrofossils indicate a thermal maximum around 11–10 cal ka BP, followed by a relatively stable and colder mean climate for the remainder of the Holocene (Shala et al., 2017). Lake Loitsana chironomid assemblages also indicate a thermal maximum at  $\sim 10$  cal ka BP (Fig. 6b), followed by cooling into the mid-Holocene and a protracted cool period from  $\sim 7.5$  to 5.5 cal ka BP, and finally a persistent warming trend from 5.5 cal ka BP to present (Shala et al., 2017). The late Holocene warming in the chironomid record is unusual compared to other high-latitude warm-season temperature reconstructions (e.g., Kaufman et al., 2020, 2016; Porter et al., 2019), which typically show long-term cooling during the late-Holocene as per summer insolation trends (Fig. 6c). Conversely, cold-season-specific Holocene temperature reconstructions from areas of Siberia (Meyer et al., 2015), Alaska (Longo et al., 2017) and north-western Canada (Holland et al., 2020) show a long-term warming trend in the late Holocene attributed to increasing winter-spring insolation trends. Regardless, the aquatic macrofossils and chironomids from Lake Loitsana both argue for an earlier Holocene thermal maximum compared to the Lake Loitsana pollen and AJU brGDGT records.

Prior to this study, the balance of evidence had suggested an early Holocene thermal maximum was more probable, and the apparent failing of the Lake Loitsana pollen record to capture an earlier thermal maximum was attributed to a possible local overrepresentation of cold-climate pollen types (e.g., Cyperaceae, Poaceae and *Equisetum*) during the early Holocene, and an overrepresentation of warmer taxa such as *Alnus* during the mid-Holocene (Shala et al., 2017). However, the presence or absence of specific terrestrial flora are unlikely drivers of lacustrine brGDGT distributions, which dominantly respond to in situ water temperature (e.g., Martínez-Sosa et al., 2021; Raberg et al., 2021; Zhao et al., 2021). The independence of the pollen and brGDGT temperature proxies and their coherence in timing and magnitude of key Holocene climatic transitions offer compelling support for this alternate version of events.

Interestingly, the dichotomous patterns of Holocene peak warmth in the pollen versus chironomid records are also repeated more broadly across northern Fennoscandia. As in northern Finland, the regional pollen composite (Fig. 7b) shows a middle Holocene thermal maximum, while the regional chironomid record (Fig. 7d) shows an early Holocene thermal maximum. This regional-scale perspective rules out local factors (e.g., lake-level effects on chironomids or overrepresentation of certain plant types in the catchment; Eggermont and Heiri, 2012; Juggins, 2013; Nyman et al., 2008; Rosén et al., 2003; Shala et al., 2017). It is likewise noteworthy that the regional diatom-temperature compilation (Fig. 7c) shows a mid-Holocene thermal maximum around 6 cal ka BP and long-term cooling thereafter, in good agreement with pollen and brGDGTs.

The seemingly paradoxical difference of chironomid- and pollen-derived temperature reconstructions in Fennoscandia is perhaps best explained by a difference in proxy seasonality. While chironomids are generally thought to reflect July temperatures (e.g., Brooks, 2006; Shala et al., 2017), pollen assemblages may capture a more integrated growing season temperature signal, similar to the MAF signal in brGDGTs. This possibility is supported by the alignment of pollen-derived temperatures and above freezing monthly (July–September) insolation curves (Fig. 6c). Furthermore, previous studies throughout the North Atlantic region also infer a dominant sensitivity of pollen to minimum monthly and growing season temperatures (Lotter et al., 2000; Marsicek et al., 2018; Williams and Shuman, 2008). In the North Atlantic region, pollen-derived reconstructions of growing degree days, similarly display relatively cold early Holocene temperatures that warm into the mid-Holocene, in agreement with simulated growing degree days using

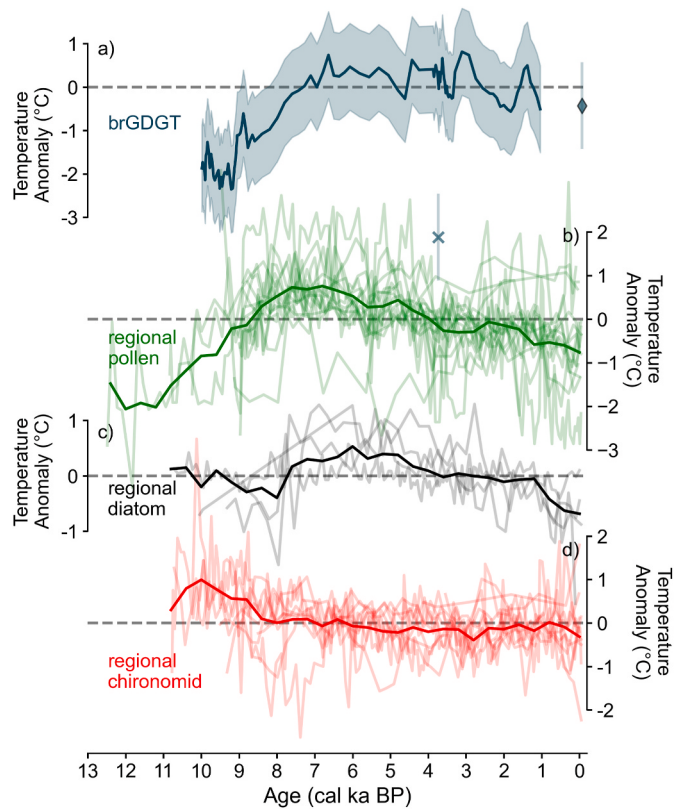


**Fig. 7.** Comparison of (a) the lake AJU brGDGT-MAF reconstruction using the ML<sub>fa</sub> transfer function (Eq. (9);  $2\sigma$  uncertainty, shaded area) with regionally averaged summer temperature reconstructions from (b) pollen, (c) diatoms, and (d) chironomids from sites across the northern Fennoscandian region. Regional averages (thick lines) are indicated for pollen, diatoms, and chironomids. Prior to averaging by proxy type, individual time-series were converted to temperature anomalies relative to their long-term mean value representing the period 8.5 cal ka BP to present that is shared by most records (refer to section 2.2 for more details).

the Community Climate System Model 3 (CCSM3; Marsicek et al., 2018).

CCSM3 simulated June–August temperatures in North America and Europe indicated an early Holocene thermal maximum followed by long-term cooling (Marsicek et al., 2018). This is significant because the model suggests that naturally occurring configurations of climate forcings and rapidly evolving deglacial boundary conditions can produce disparate Holocene climate trends and thermal maxima depending on seasonality (Marsicek et al., 2018).

As a regionally novel proxy, the brGDGT record from lake AJU provides valuable insight into the potential significance of proxy seasonality when reconstructing past climate conditions. BrGDGTs, pollen, diatoms, and chironomids are associated with unique strengths and together provide a more holistic understanding of paleoclimate changes. A continued diversification of the temperature-proxy network is expected to bring more clarity to the subject of Holocene thermal maximum timing in this region and help to pinpoint causes of inter-proxy differences.

#### 4. Conclusions

A  $\sim 9.0$  kyr record of MAF was reconstructed from brGDGTs in Lake AJU, northern Finland, using a newly developed, high-latitude lake-specific transfer function. Reconstructed temperatures indicate a cool early Holocene that warmed into the mid-Holocene. Warm conditions persisted through the mid-Holocene, which is unique to north-eastern Fennoscandia, and then cooled throughout the late Holocene. The

brGDGT temperature proxy exhibits a probable bias towards warm-season temperatures in this region given the good agreement with modern mean monthly temperatures above freezing and June–September insolation patterns. Regionally, pollen and diatom climate proxies also show a mid-Holocene thermal maximum, in agreement with the AJU brGDGT record, which suggests a possible bias toward warm- or growing-season conditions. In contrast, the early Holocene thermal maximum reconstructed by some aquatic macrofossil records and many chironomid records across northern Fennoscandia is more consistent with early summer (e.g., June–July) insolation trends. Proxy-specific seasonality biases offer a tenable explanation for the apparent discrepancy in the timing of peak Holocene temperatures observed among the primary biological proxies employed in Fennoscandia. However, environmental sensitivities of these proxies to other factors such as lake level or water quality may also contribute to this disparity. Future efforts to expand the network of climate proxy reconstructions in Fennoscandia, with a particular emphasis on lake sediment archives, will improve our understanding of the climatic and environmental drivers of variability in these proxies. This, in turn, will enable more accurate and nuanced interpretations of Holocene climate dynamics in Fennoscandia.

## Author contributions

**Gerard Otiniano:** methodology, formal analysis, investigation, writing – original draft, and visualization. **Trevor J. Porter:** conceptualization, methodology, writing – original draft, writing – review and editing, supervision, funding acquisition. **Michael Phillips:** methodology, formal analysis, writing – review and editing. **Sari Juutinen:** conceptualization, investigation, writing – review and editing. **Jan Weckström:** conceptualization, investigation, writing – review and editing. **Maija Heikkilä:** conceptualization, supervision, investigation, funding acquisition, methodology, writing – review and editing.

## Declaration of competing interest

The authors declare that they have no known competing financial interests or personal relationships that could have appeared to influence the work reported in this paper.

## Data availability

The data is included in the submission for review but will be published in an online repository.

## Acknowledgements

Funding for this project was provided by NSERC Discovery Grants to TP (RGPIN-2016-06730) and MP (RGPIN-2017-06400) and Academy of Finland Grants to MH (296423, 334509) and funding for infrastructure was obtained from the Canadian Foundation for Innovation-Ontario Research Fund John Evans Leaders Fund to TP (Project # 34864) and MP (Project # 36131). The authors also thank Patrick Rioual, editor for QSR, as well as reviewers Jonathan Raberg and the two anonymous reviewers for their thoughtful feedback which improved the manuscript.

## Appendix A. Supplementary data

Supplementary data to this article can be found online at <https://doi.org/10.1016/j.quascirev.2024.108555>.

## References

- Aa, A.R., Sønstegaard, E., 2019. Early-Holocene glacier fluctuations of northern Grovabreen, western Norway. *Holocene* 29, 187–196. <https://doi.org/10.1177/0959683618810392>.
- Andersen, C., Koç, N., Jennings, A., Andrews, J.T., 2004. Nonuniform response of the major surface currents in the Nordic Seas to insolation forcing: implications for the Holocene climate variability. *Paleoceanography* 19. <https://doi.org/10.1029/2002PA000873>.
- Autio, J., Hicks, S., 2004. Annual variations in pollen deposition and meteorological conditions on the fell Aakenustunturi in northern Finland: potential for using fossil pollen as a climate proxy. *Grana* 43, 31–47. <https://doi.org/10.1080/00173130310017409>.
- Baxter, A.J., Hopmans, E.C., Russell, J.M., Sinnighé Damsté, J.S., 2019. Bacterial GMGTs in East African lake sediments: their potential as palaeotemperature indicators. *Geochem. Cosmochim. Acta* 259, 155–169. <https://doi.org/10.1016/j.gca.2019.05.039>.
- Baxter, A.J., van Bree, L.G.J., Peterse, F., Hopmans, E.C., Villanueva, L., Verschuren, D., Sinnighé Damsté, J.S., 2021. Seasonal and multi-annual variation in the abundance of isoprenoid GDGT membrane lipids and their producers in the water column of a meromictic equatorial crater lake (Lake Chala, East Africa). *Quat. Sci. Rev.* 273, 107263 <https://doi.org/10.1016/j.quascirev.2021.107263>.
- Bechtel, A., Smittenberg, R.H., Bernasconi, S.M., Schubert, C.J., 2010. Distribution of branched and isoprenoid tetraether lipids in an oligotrophic and a eutrophic Swiss lake: insights into sources and GDGT-based proxies. *Org. Geochem.* 41, 822–832. <https://doi.org/10.1016/j.orggeochem.2010.04.022>.
- Bigler, C., Hall, R.I., 2003. Diatoms as quantitative indicators of July temperature: a validation attempt at century-scale with meteorological data from northern Sweden. *Palaeogeogr. Palaeoclimatol. Palaeoecol.* 189, 147–160. [https://doi.org/10.1016/S0031-0182\(02\)00638-7](https://doi.org/10.1016/S0031-0182(02)00638-7).
- Blaauw, M., Christen, J.A., 2011. Flexible paleoclimate age-depth models using an autoregressive gamma process. *Bayesian Anal.* 6, 457–474. <https://doi.org/10.1214/11-BA618>.
- Brooks, S.J., 2006. Fossil midges (Diptera: Chironomidae) as palaeoclimatic indicators for the Eurasian region. *Quat. Sci. Rev.*, Quater. Beetle Res.: State Art 25, 1894–1910. <https://doi.org/10.1016/j.quascirev.2005.03.021>.
- Cao, M., Rivas-Ruiz, P., Trapote, M., del, C., Vegas-Vilarrubia, T., Rull, V., Rosell-Melé, A., 2020. Seasonal effects of water temperature and dissolved oxygen on the isoGDGT proxy (TEX86) in a Mediterranean oligotrophic lake. *Chem. Geol.* 551, 119759 <https://doi.org/10.1016/j.chemgeo.2020.119759>.
- Cartapanis, O., Jonkers, I., Moffa-Sánchez, P., Jaccard, S.L., de Vernal, A., 2022. Complex spatio-temporal structure of the Holocene thermal maximum. *Nat. Commun.* 13, 5662. <https://doi.org/10.1038/s41467-022-33362-1>.
- Chen, Y., Zheng, F., Yang, H., Wang, W., Wu, Liu, X., Liang, H., Chen, H., Pei, H., Zhang, C., Pancost, R.D., Zeng, Z., 2022. The production of diverse brGDGTs by an Acidobacterium allows a direct test of temperature and pH controls on their distribution. *bioRxiv* 2022.04.07.487437. <https://doi.org/10.1101/2022.04.07.487437>.
- Dahl, S.O., Nesje, A., Lie, Ø., Fjordheim, K., Matthews, J.A., 2002. Timing, equilibrium-line altitudes and climatic implications of two early-Holocene glacier readvances during the Erdalen Event at Jostedalsbreen, western Norway. *Holocene* 12, 17–25. <https://doi.org/10.1191/0959683602hl516rp>.
- Dang, X., Ding, W., Yang, H., Pancost, R.D., Naafs, B.D.A., Xue, J., Lin, X., Lu, J., Xie, S., 2018. Different temperature dependence of the bacterial brGDGT isomers in 35 Chinese lake sediments compared to that in soils. *Org. Geochem.* 119, 72–79. <https://doi.org/10.1016/j.orggeochem.2018.02.008>.
- De Jonge, C., Hopmans, E.C., Stadnitskaia, A., Rijpstra, W.I.C., Hofland, R., Tegelaar, E., Sinnighé Damsté, J.S., 2013. Identification of novel penta- and hexamethylated branched glycerol dialkyl glycerol tetraethers in peat using HPLC-MS<sub>2</sub>, GC-MS and GC-SMB-MS. *Org. Geochem.* 54, 78–82. <https://doi.org/10.1016/j.orggeochem.2012.10.004>.
- De Jonge, C., Hopmans, E.C., Zell, C.I., Kim, J.-H., Schouten, S., Sinnighé Damsté, J.S., 2014. Occurrence and abundance of 6-methyl branched glycerol dialkyl glycerol tetraethers in soils: implications for palaeoclimate reconstruction. *Geochim. Cosmochim. Acta* 141, 97–112. <https://doi.org/10.1016/j.gca.2014.06.013>.
- De Jonge, C., Radujković, D., Sigurdsson, B.D., Weedon, J.T., Janssens, I., Peterse, F., 2019. Lipid biomarker temperature proxy responds to abrupt shift in the bacterial community composition in geothermally heated soils. *Org. Geochem.* 137, 103897 <https://doi.org/10.1016/j.orggeochem.2019.07.006>.
- De Jonge, C., Stadnitskaia, A., Hopmans, E.C., Cherkashov, G., Fedotov, A., Streletskaia, I.D., Vasiliev, A.A., Sinnighé Damsté, J.S., 2015. Drastic changes in the distribution of branched tetraether lipids in suspended matter and sediments from the Yenisei River and Kara Sea (Siberia): implications for the use of brGDGT-based proxies in coastal marine sediments. *Geochim. Cosmochim. Acta* 165, 200–225. <https://doi.org/10.1016/j.gca.2015.05.044>.
- Ding, S., Xu, Y., Wang, Y., He, Y., Hou, J., Chen, L., He, J.-S., 2015. Distribution of branched glycerol dialkyl glycerol tetraethers in surface soils of the Qinghai-Tibetan Plateau: implications of brGDGTs-based proxies in cold and dry regions. *Biogeosciences* 12, 3141–3151. <https://doi.org/10.5194/bg-12-3141-2015>.
- Duplessy, J.C., Cortijo, E., Ivanova, E., Khusid, T., Labeyrie, L., Levitan, M., Murdmaa, I., Paterné, M., 2005. Paleoceanography of the Barents Sea during the Holocene. *Paleoceanography* 20. <https://doi.org/10.1029/2004PA001116>.
- Eggermont, H., Heiri, O., 2012. The chironomid-temperature relationship: expression in nature and palaeoenvironmental implications. *Biol. Rev.* 87, 430–456. <https://doi.org/10.1111/j.1469-185X.2011.00206.x>.
- Elson, P., Andrade, E.S. de, Lucas, G., May, R., Hattersley, R., Campbell, E., Dawson, A., Raynaud, S., Little, B., Snow, A.D., Donkers, K., Blay, B., Killick, P., Wilson, N., Peglar, P., Ibdreyer, Andrew, Szymaniak, J., Berchet, A., Bosley, C., Davis, L., Filipe, Krasting, J., Bradbury, M., Kirkham, D., Stephenworsley, Clément, Caria, G., Hedley, M., 2022. SciTools/cartopy: v0.21.0. <https://doi.org/10.5281/zenodo.7065949>.

- England, M.R., Eisenman, I., Lutsko, N.J., Wagner, T.J.W., 2021. The recent emergence of arctic amplification. *Geophys. Res. Lett.* 48, e2021GL094086 <https://doi.org/10.1029/2021GL094086>.
- Foley, J.A., Kutzbach, J.E., Coe, M.T., Levis, S., 1994. Feedbacks between climate and boreal forests during the Holocene epoch. *Nature* 371, 52–54. <https://doi.org/10.1038/371052a0>.
- Halamka, T.A., Raberg, J.H., McFarlin, J.M., Younkin, A.D., Mulligan, C., Liu, X.-L., Kopf, S.H., 2022. Production of diverse brGDGTs by *Acidobacterium Solibacter usitatus* in response to temperature, pH, and O<sub>2</sub> provides a culturing perspective on brGDGT proxies and biosynthesis. *Geobiology*. <https://doi.org/10.1111/gbi.12525>.
- Harning, D.J., Curtin, L., Geirsdóttir, A., D'Andrea, W.J., Miller, G.H., Sepúlveda, J., 2020. Lipid biomarkers quantify Holocene summer temperature and ice cap sensitivity in Icelandic lakes. *Geophys. Res. Lett.* 47, e2019GL085728 <https://doi.org/10.1029/2019GL085728>.
- Harris, C.R., Millman, K.J., van der Walt, S.J., Gommers, R., Virtanen, P., Cournapeau, D., Wieser, E., Taylor, J., Berg, S., Smith, N.J., Kern, R., Picus, M., Hoyer, S., van Kerckwijk, M.H., Brett, M., Haldane, A., del Río, J.F., Wiebe, M., Peterson, P., Gérard-Marchant, P., Sheppard, K., Reddy, T., Weckesser, W., Abbasi, H., Gohlke, C., Oiphant, T.E., 2020. Array programming with NumPy. *Nature* 585, 357–362. <https://doi.org/10.1038/s41586-020-2649-2>.
- Hersbach, H., Bell, B., Berrisford, P., Hirahara, S., Horányi, A., Muñoz-Sabater, J., Nicolas, J., Peubey, C., Radu, R., Schepers, D., Simmons, A., Soci, C., Abdalla, S., Abellán, X., Balsamo, G., Bechtold, P., Biavati, G., Bidlot, J., Bonavita, M., De Chiara, G., Dahlgren, P., Dee, D., Diamantakis, M., Dragani, R., Flemming, J., Forbes, R., Fuentes, M., Geer, A., Haimberger, L., Healy, S., Hogan, R.J., Hólm, E., Janisková, M., Keeley, S., Laloyaux, P., Lopez, P., Lupu, C., Radnoti, G., de Rosnay, P., Rozum, I., Vamborg, F., Villaume, S., Thépaut, J.-N., 2020. The ERA5 global reanalysis. *Q. J. R. Meteorol. Soc.* 146, 1999–2049. <https://doi.org/10.1002/qj.3803>.
- Holland, K.M., Porter, T.J., Froese, D.G., Kokelj, S.V., Buchanan, C.A., 2020. Ice-wedge evidence of Holocene winter warming in the Canadian arctic. *Geophys. Res. Lett.* 47, e2020GL087942 <https://doi.org/10.1029/2020GL087942>.
- Hopmans, E.C., Schouten, S., Sinninghe Damsté, J.S., 2016. The effect of improved chromatography on GDGT-based palaeoproxies. *Org. Geochem.* 93, 1–6. <https://doi.org/10.1016/j.orggeochem.2015.12.006>.
- Hopmans, E.C., Weijers, J.W.H., Scheubel, E., Herfort, L., Sinninghe Damsté, J.S., Schouten, S., 2004. A novel proxy for terrestrial organic matter in sediments based on branched and isoprenoid tetraether lipids. *Earth Planet Sci. Lett.* 224, 107–116. <https://doi.org/10.1016/j.epsl.2004.05.012>.
- Huang, J., Zhang, X., Zhang, Q., Lin, Y., Hao, M., Luo, Y., Zhao, Z., Yao, Y., Chen, X., Wang, L., Nie, S., Yin, Y., Xu, Y., Zhang, J., 2017. Recently amplified arctic warming has contributed to a continual global warming trend. *Nat. Clim. Change* 7, 875–879. <https://doi.org/10.1038/s41558-017-0009-5>.
- Juggins, S., 2013. Quantitative reconstructions in palaeolimnology: new paradigm or sick science? *Quat. Sci. Rev.* 64, 20–32. <https://doi.org/10.1016/j.quascirev.2012.12.014>.
- Kaniewski, D., Marriner, N., Cheddadi, R., Morhange, C., Ontiveros, M.Á.C., Fornós, J.J., Giaime, M., Trichon, V., Otto, T., Luce, F., Van Campo, E., 2020. Recent anthropogenic climate change exceeds the rate and magnitude of natural Holocene variability on the Balearic Islands. *Anthropocene* 32, 100268. <https://doi.org/10.1016/j.anocene.2020.100268>.
- Kaufman, D.S., Axford, Y.L., Henderson, A.C.G., McKay, N.P., Oswald, W.W., Saenger, C., Anderson, R.S., Bailey, H.L., Clegg, B., Gajewski, K., Hu, F.S., Jones, M.C., Massa, C., Routson, C.C., Werner, A., Wooller, M.J., Yu, Z., 2016. Holocene climate changes in eastern Beringia (NW North America) – a systematic review of multi-proxy evidence. *Quat. Sci. Rev.* 147, 312–339. <https://doi.org/10.1016/j.quascirev.2015.10.021>.
- Kaufman, D.S., Broadman, 2023. Revisiting the Holocene global temperature conundrum. *Nature* 614, 425–435. <https://doi.org/10.1038/s41586-022-05536-w>.
- Kaufman, D.S., McKay, N., Routson, C., Erb, M., Dätwyler, C., Sommer, P.S., Heiri, O., Davis, B., 2020. Holocene global mean surface temperature, a multi-method reconstruction approach. *Sci. Data* 7, 201. <https://doi.org/10.1038/s41597-020-0530-7>.
- Khider, D., Emile-Geay, J., Zhu, F., James, A., Landers, J., Kwan, M., Athreya, P., 2022. Pyleoclim: A Python Package for the Analysis and Visualization of Paleoclimate Data. <https://doi.org/10.5281/ZENODO.1205661>.
- Korholha, A., Ruppel, M., Seppä, H., Välijanta, M., Virtanen, T., Weckström, J., 2010. The importance of northern peatland expansion to the late-Holocene rise of atmospheric methane. *Quat. Sci. Rev.* 29, 611–617. <https://doi.org/10.1016/j.quascirev.2009.12.010>.
- Larocque, I., Hall, R.I., 2004. Holocene temperature estimates and chironomid community composition in the Abisko Valley, northern Sweden. *Quat. Sci. Rev.* 23, 2453–2465. <https://doi.org/10.1016/j.quascirev.2004.04.006>.
- Laskar, J., Robutel, P., Joutel, F., Gastineau, M., Correia, A.C.M., Levrard, B., 2004. A long-term numerical solution for the insolation quantities of the Earth. *Astron. Astrophys.* 428, 261–285. <https://doi.org/10.1051/0004-6361:20041335>.
- Longo, W.M., Huang, Y., Russell, J.M., Morrill, C., Daniels, W., Giblin, A.E., Crowther, J., 2017. A high-resolution lacustrine alkenone record demonstrates progressive cold season warming during the Holocene in arctic Alaska. In: AGU Fall Meeting Abstracts 54.
- Lotter, A.F., Birks, H.J.B., Eicher, U., Hofmann, W., Schwander, J., Wick, L., 2000. Younger Dryas and Allerød summer temperatures at Gerzensee (Switzerland) inferred from fossil pollen and cladoceran assemblages. *Palaeogeogr. Palaeoclimatol. Palaeoecol.* 159, 349–361. [https://doi.org/10.1016/S0031-0182\(00\)00093-6](https://doi.org/10.1016/S0031-0182(00)00093-6).
- Marcott, S.A., Shakun, J.D., Clark, P.U., Mix, A.C., 2013. A reconstruction of regional and global temperature for the past 11,300 years. *Science* 339, 1198–1201. <https://doi.org/10.1126/science.1228026>.
- Marsicek, J., Shuman, B.N., Bartlein, P.J., Shafer, S.L., Brewer, S., 2018. Reconciling divergent trends and millennial variations in Holocene temperatures. *Nature* 554, 92–96. <https://doi.org/10.1038/nature25464>.
- Martin, C., Ménot, G., Thouveny, N., Davtian, N., Andreu-Ponel, V., Reille, M., Bard, E., 2019. Impact of human activities and vegetation changes on the tetraether sources in Lake St Front (Massif Central, France). *Org. Geochem.* 135, 38–52. <https://doi.org/10.1016/j.orggeochem.2019.06.005>.
- Martínez-Sosa, P., Tierney, J.E., Meredith, L.K., 2020. Controlled lacustrine microcosms show a brGDGT response to environmental perturbations. *Org. Geochem.*, 104041 <https://doi.org/10.1016/j.orggeochem.2020.104041>.
- Martínez-Sosa, P., Tierney, J.E., Pérez-Angel, L.C., Stefanescu, I.C., Guo, J., Kirkels, F., Sepúlveda, J., Peterse, F., Shuman, B.N., Reyes, A.V., 2023. Development and application of the branched and isoprenoid GDGT machine learning classification algorithm (BIGMaC) for paleoenvironmental reconstruction. *Paleoceanogr. Paleoclimatol.* 38, e2023PA004611 <https://doi.org/10.1029/2023PA004611>.
- Martínez-Sosa, P., Tierney, J.E., Stefanescu, I.C., Dearing Crampton-Flood, E., Shuman, B.N., Routsos, C., 2021. A global Bayesian temperature calibration for lacustrine brGDGTs. *Geochem. Cosmochim. Acta* 305, 87–105. <https://doi.org/10.1016/j.gca.2021.04.038>.
- Matthews, J.A., Dresser, P.Q., 2008. Holocene glacier variation chronology of the Smørstabbtindan massif, Jotunheimen, southern Norway, and the recognition of century- to millennial-scale European Neoglacial Events. *Holocene* 18, 181–201. <https://doi.org/10.1177/0959683607085608>.
- McKinney, W., 2010. Data structures for statistical computing in Python. In: Presented at the Python in Science Conference, Austin, Texas, pp. 56–61. <https://doi.org/10.25080/Majora-92bf1922-00a>.
- Meyer, H., Opel, T., Laepple, T., Dereviagin, A.Y., Hoffmann, K., Werner, M., 2015. Long-term winter warming trend in the Siberian Arctic during the mid- to late Holocene. *Nat. Geosci.* 8, 122–125. <https://doi.org/10.1038/ngeo2349>.
- Naafs, B.D.A., Gallego-Sala, A.V., Inglis, G.N., Pancost, R.D., 2017. Refining the global branched glycerol dialkyl glycerol tetraether (brGDGT) soil temperature calibration. *Org. Geochem.* 106, 48–56. <https://doi.org/10.1016/j.orggeochem.2017.01.009>.
- Naehler, S., Peterse, F., Smittenberg, R.H., Niemann, H., Zigah, P.K., Schubert, C.J., 2014. Sources of glycerol dialkyl glycerol tetraethers (GDGTs) in catchment soils, water column and sediments of Lake Rotsee (Switzerland) – implications for the application of GDGT-based proxies for lakes. *Org. Geochem.* 66, 164–173. <https://doi.org/10.1016/j.orggeochem.2013.10.017>.
- Nesje, A., 2009. Latest pleistocene and Holocene alpine glacier fluctuations in Scandinavia. *Quat. Sci. Rev.*, Holocene Latest Pleistocene Alpine Glacier Fluctuations: Global Perspect. 28, 2119–2136. <https://doi.org/10.1016/j.quascirev.2008.12.016>.
- Nesje, A., Bjune, A.E., Bakke, J., Dahl, S.O., Lie, Ø., Birks, H.J.B., 2006. Holocene palaeoclimate reconstructions at Vanndalsvatnet, western Norway, with particular reference to the 8200 cal. yr BP event. *Holocene* 16, 717–729. <https://doi.org/10.1191/0959683606hl954rp>.
- Nym, M., Weckström, J., Korholha, A., 2008. Chironomid response to environmental drivers during the Holocene in a shallow treeline lake in northwestern Fennoscandia. *Holocene* 18, 215–227. <https://doi.org/10.1177/0959683607086760>.
- O'Beirne, M.D., Scott, W.P., Werne, J.P., 2023. A critical assessment of lacustrine branched glycerol dialkyl glycerol tetraether (brGDGT) temperature calibration models. *Geochem. Cosmochim. Acta* 359, 100–118. <https://doi.org/10.1016/j.gca.2023.08.019>.
- Otiniano, G.A., Porter, T.J., Benowitz, J.A., Bindeman, I.N., Froese, D.G., Jensen, B.J.L., Davies, L.J., Phillips, M.A., 2020. A late miocene to late pleistocene reconstruction of precipitation isotopes and climate from hydrated volcanic glass shards and biomarkers in central Alaska and Yukon. *Paleoceanogr. Paleoclimatol.* 35, e2019PA003791 <https://doi.org/10.1029/2019PA003791>.
- Otiniano, G.A., Porter, T.J., Buceta, R.E., Bergman, M.E., Phillips, M.A., 2023. Climatic and environmentally driven variability in lacustrine brGDGT distributions at local to regional scales in Alaska and northwestern Canada. *Org. Geochem.* 181, 104604 <https://doi.org/10.1016/j.orggeochem.2023.104604>.
- Parish, M., Du, X., Bijaksana, S., Russell, J., 2023. A brGDGT-based reconstruction of terrestrial temperature from the maritime continent spanning the last glacial maximum. *Paleoceanogr. Paleoclimatol.* 38 <https://doi.org/10.1029/2022PA004501>.
- Paus, A., Haflidason, H., Routh, J., Naafs, B.D.A., Thoen, M.W., 2019. Environmental responses to the 9.7 and 8.2 cold events at two ecolonal sites in the Dovre mountains, mid-Norway. *Quat. Sci. Rev.* 205, 45–61. <https://doi.org/10.1016/j.quascirev.2018.12.009>.
- Paus, A., Velle, G., Larsen, J., Lie, Ø., Nesje, A., 2006. Lateglacial nunataks in central Scandinavia: biostratigraphical evidence for ice thickness from Lake Flåfjattjønn, Tynset, Norway. *Quat. Sci. Rev.* 25, 1228–1246. <https://doi.org/10.1016/j.quascirev.2005.10.008>.
- Pearce, M.D., Beverly, E.J., Garza, B., Baker, S., Levin, N.E., Tierney, J.E., Hägg, C., Feakins, S.J., 2022. Identifying the drivers of GDGT distributions in alkaline soil profiles within the Serengeti ecosystem. *Org. Geochem.* 169, 104433 <https://doi.org/10.1016/j.orggeochem.2022.104433>.
- Pearson, E.J., Juggins, S., Talbot, H.M., Weckström, J., Rosén, P., Ryves, D.B., Roberts, S.J., Schmidt, R., 2011. A lacustrine GDGT-temperature calibration from the Scandinavian Arctic to Antarctic: renewed potential for the application of GDGT-paleothermometry in lakes. *Geochem. Cosmochim. Acta* 75, 6225–6238. <https://doi.org/10.1016/j.gca.2011.07.042>.
- Pérez-Angel, L.C., Sepúlveda, J., Molnar, P., Montes, C., Rajagopalan, B., Snell, K., Gonzalez-Arango, C., Dildar, N., 2020. Soil and air temperature calibrations using branched GDGTs for the tropical Andes of Colombia: toward a Pan-tropical

- calibration. *Geochem., Geophys., Geosyst.* 21, e2020GC008941 <https://doi.org/10.1029/2020GC008941>.
- Porter, T.J., Schoenemann, S.W., Davies, L.J., Steig, E.J., Bandara, S., Froese, D.G., 2019. Recent summer warming in northwestern Canada exceeds the Holocene thermal maximum. *Nat. Commun.* 10, 10. <https://doi.org/10.1038/s41467-019-09622-y>.
- Previdi, M., Smith, K.L., Polvani, L.M., 2021. Arctic amplification of climate change: a review of underlying mechanisms. *Environ. Res. Lett.* 16, 093003 <https://doi.org/10.1088/1748-9326/ac1c29>.
- Qian, S., Yang, H., Dong, C., Wang, Y., Wu, J., Pei, H., Dang, X., Lu, J., Zhao, S., Xie, S., 2019. Rapid response of fossil tetraether lipids in lake sediments to seasonal environmental variables in a shallow lake in central China: implications for the use of tetraether-based proxies. *Org. Geochem.* 128, 108–121. <https://doi.org/10.1016/j.orggeochem.2018.12.007>.
- Raberg, J.H., Flores, E., Crump, S.E., de Wet, G., Dildar, N., Miller, G.H., Geirsdóttir, Á., Sepúlveda, J., 2022a. Intact polar brGDGTs in arctic lake catchments: implications for lipid sources and paleoclimate applications. *J. Geophys. Res.: Biogeosci.* 127, e2022JG006969. <https://doi.org/10.1029/2022JG006969>.
- Raberg, J.H., Harning, D.J., Crump, S.E., de Wet, G., Blumm, A., Kopf, S., Geirsdóttir, Á., Miller, G.H., Sepúlveda, J., 2021. Revised fractional abundances and warm-season temperatures substantially improve brGDGT calibrations in lake sediments. *Biogeosciences* 18, 3579–3603. <https://doi.org/10.5194/bg-18-3579-2021>.
- Raberg, J.H., Miller, G.H., Geirsdóttir, Á., Sepúlveda, J., 2022b. Near-universal trends in brGDGT lipid distributions in nature. *Sci. Adv.* 8, eabm7625 <https://doi.org/10.1126/sciadv.abm7625>.
- Rantanen, M., Karpechko, A.Yu., Lipponen, A., Nordling, K., Hyvärinen, O., Ruosteenoja, K., Vihma, T., Laaksonen, A., 2022. The Arctic has warmed nearly four times faster than the globe since 1979. *Commun. Earth Environ.* 3, 168. <https://doi.org/10.1038/s43247-022-00498-3>.
- Reback, J., Jbrockmendel, McKinney, W., Van Den Bossche, J., Roeschke, M., Augspurger, T., Hawkins, S., Cloud, P., Gfyong Hoefer, P., Sinhrks, Klein, A., Petersen, T., Tratner, J., She, C., Ayd, W., Shadrach, R., Naveh, S., Garcia, M., Derbyshire, J.H.M., Schendel, J., Wörtwein, T., Hayden, A., Saxton, D., Gorelli, M.E., Li, F., Zeitlin, M., Jancauskas, V., McMaster, A., Li, T., 2022. Pandas-Dev/Pandas: Pandas 1.4.4. <https://doi.org/10.5281/ZENODO.3509134>.
- Rehfeld, K., Marwan, N., Heitzig, J., Kurths, J., 2011. Comparison of correlation analysis techniques for irregularly sampled time series. *Nonlinear Process Geophys.* 18, 389–404. <https://doi.org/10.5194/npg-18-389-2011>.
- Reimer, P.J., Austin, W.E.N., Bard, E., Bayliss, A., Blackwell, P.G., Bronk Ramsey, C., Butzin, M., Cheng, H., Edwards, R.L., Friedrich, M., Grootes, P.M., Guilderson, T.P., Hajdas, I., Heaton, T.J., Hogg, A.G., Hughen, K.A., Kromer, B., Manning, S.W., Muscheler, R., Palmer, J.G., Pearson, C., Van Der Plicht, J., Reimer, R.W., Richards, D.A., Scott, E.M., Southon, J.R., Turney, C.S.M., Wacker, L., Adolphi, F., Büntgen, U., Capron, M., Fahrni, S.M., Fogtmann-Schulz, A., Friedrich, R., Köhler, P., Kudsk, S., Miyake, F., Olsen, J., Reining, F., Sakamoto, M., Sookdeo, A., Talamo, S., 2020. The IntCal20 northern Hemisphere radiocarbon age calibration curve (0–55 cal kBP). *Radiocarbon* 62, 725–757. <https://doi.org/10.1017/RDC.2020.41>.
- Renberg, I., Hannson, H., 2008. The HTH sediment corer. *J. Paleolimnol.* 40, 655–659. <https://doi.org/10.1007/s10933-007-9188-9>.
- Renssen, H., Seppä, H., Crosta, X., Goosse, H., Roche, D.M., 2012. Global characterization of the Holocene thermal maximum. *Quat. Sci. Rev.* 48, 7–19. <https://doi.org/10.1016/j.quascirev.2012.05.022>.
- Rosén, P., Segerström, U., Eriksson, L., Renberg, I., 2003. Do diatom, chironomid, and pollen records consistently infer Holocene July air temperature? A comparison using sediment cores from four Alpine lakes in northern Sweden. *Arctic Antarct. Alpine Res.* 35, 279–290. [https://doi.org/10.1657/1523-0430\(2003\)035\[0279:DDCAPR\]2.0.CO;2](https://doi.org/10.1657/1523-0430(2003)035[0279:DDCAPR]2.0.CO;2).
- Ruddiman, W.F., Fuller, D.Q., Kutzbach, J.E., Tzedakis, P.C., Kaplan, J.O., Ellis, E.C., Vavrus, S.J., Roberts, C.N., Fyfe, R., He, F., Lemmen, C., Woodbridge, J., 2016. Late Holocene climate: natural or anthropogenic? *Rev. Geophys.* 54, 93–118. <https://doi.org/10.1002/2015RG000503>.
- Russell, J.M., Hopmans, E.C., Loomis, S.E., Liang, J., Sinninge Damsté, J.S., 2018. Distributions of 5- and 6-methyl branched glycerol dialkyl glycerol tetraethers (brGDGTs) in East African lake sediment: effects of temperature, pH, and new lacustrine paleotemperature calibrations. *Org. Geochem.* 117, 56–69. <https://doi.org/10.1016/j.orggeochem.2017.12.003>.
- Sejrup, H.P., Seppä, H., McKay, N.P., Kaufman, D.S., Geirsdóttir, Á., de Vernal, A., Renssen, H., Husum, K., Jennings, A., Andrews, J.T., 2016. North Atlantic–Fennoscandian Holocene climate trends and mechanisms. *Quat. Sci. Rev.* 147, 365–378. <https://doi.org/10.1016/j.quascirev.2016.06.005>.
- Seppä, H., Bjune, A.E., Telford, R.J., Birks, H.J.B., Veski, S., 2009. Last nine-thousand years of temperature variability in Northern Europe. *Clim. Past* 5, 523–535. <https://doi.org/10.5194/cp-5-523-2009>.
- Serreze, M.C., Barry, R.G., 2011. Processes and impacts of Arctic amplification: a research synthesis. *Global Planet. Change* 77, 85–96. <https://doi.org/10.1016/j.gloplacha.2011.03.004>.
- Shakesby, R.A., Matthews, J.A., Winkler, S., Fabel, D., Dresser, P.Q., 2020. Early-Holocene moraine chronology, Sognefjell area, southern Norway: evidence for multiple glacial and climatic fluctuations within the Erdalen Event (~10.2–9.7 ka). *Norw. J. Geol.* <https://doi.org/10.17850/njg100-3-2>.
- Shala, S., Helmens, K.F., Luoto, T.P., Salonen, J.S., Välijanta, M., Weckström, J., 2017. Comparison of quantitative Holocene temperature reconstructions using multiple proxies from a northern boreal lake. *Holocene* 27, 1745–1755. <https://doi.org/10.1177/0959683617708442>.
- Sinninghe Damsté, J.S., Hopmans, E.C., Pancost, R.D., Schouten, S., Geenevasen, J.A.J., 2000. Newly discovered non-isoprenoid glycerol dialkylglycerol tetraether lipids in sediments. *Chem. Commun.* 1683–1684. <https://doi.org/10.1039/B0045171>.
- Sinninghe Damsté, J.S., Ossebaar, J., Abbas, B., Schouten, S., Verschuren, D., 2009. Fluxes and distribution of tetraether lipids in an equatorial African lake: constraints on the application of the TEX86 palaeothermometer and BIT index in lacustrine settings. *Geochim. Cosmochim. Acta* 73, 4232–4249. <https://doi.org/10.1016/j.gca.2009.04.022>.
- Sinninghe Damsté, J.S., Rijpstra, W.I.C., Foesel, B.U., Huber, K.J., Overmann, J., Nakagawa, S., Kim, J.J., Dunfield, P.F., Dedysh, S.N., Villanueva, L., 2018. An overview of the occurrence of ether- and ester-linked iso-diabolic acid membrane lipids in microbial cultures of the Acidobacteria: implications for brGDGT paleoproxies for temperature and pH. *Org. Geochem.* 124, 63–76. <https://doi.org/10.1016/j.orggeochem.2018.07.006>.
- Sinninghe Damsté, J.S., Rijpstra, W.I.C., Hopmans, E.C., Weijers, J.W.H., Foesel, B.U., Overmann, J., Dedysh, S.N., 2011. 13,16-Dimethyl octacosanediolic acid (iso-Diabolic acid), a common membrane-spanning lipid of acidobacteria subdivisions 1 and 3. *Appl. Environ. Microbiol.* 77, 4147–4154. <https://doi.org/10.1128/AEM.00466-11>.
- Sjögren, P.J.E., 2021. An overview of Holocene climate reconstructions in northernmost Fennoscandia. *Septentrio Rep.* <https://doi.org/10.7557/7.5747>.
- Stroeven, A., Hätestrand, C., Kleman, J., Heyman, J., Fabel, D., Fredin, O., Goodfellow, B., Harbor, J., Jansen, J., Olsen, L., Caffee, M., Fink, D., Lundqvist, J., Rosqvist, G., Strömberg, B., Jansson, K., 2016. Deglaciation of Fennoscandia. *Quat. Sci. Rev.* 147, 91–121. <https://doi.org/10.1016/j.quascirev.2015.09.016>.
- Välijanta, M., Salonen, J.S., Heikkilä, M., Amon, L., Helmens, K., Klimaschewski, A., Kuhry, P., Kultti, S., Poska, A., Shala, S., Veski, S., Birks, H.H., 2015. Plant macrofossil evidence for an early onset of the Holocene summer thermal maximum in northernmost Europe. *Nat. Commun.* 6, 6809. <https://doi.org/10.1038/ncomms7809>.
- van Bree, L.G.J., Peterse, F., Baxter, A.J., De Crop, W., van Grinsven, S., Villanueva, L., Verschuren, D., Sinninge Damsté, J.S., 2020. Seasonal variability and sources of in situ brGDGT production in a permanently stratified African crater lake. *Biogeosciences* 17, 5443–5463. <https://doi.org/10.5194/bg-17-5443-2020>.
- Wanner, H., Solomina, O., Grosjean, M., Ritz, S.P., Jetel, M., 2011. Structure and origin of Holocene cold events. *Quat. Sci. Rev.* 30, 3109–3123. <https://doi.org/10.1016/j.quascirev.2011.07.010>.
- Webb, E.E., Loranty, M.M., Lichstein, J.W., 2021. Surface water, vegetation, and fire as drivers of the terrestrial Arctic-boreal albedo feedback. *Environ. Res. Lett.* 16, 084046. <https://doi.org/10.1088/1748-9326/ac4eaa>.
- Weckström, J., Seppä, H., Korhola, A., 2010. Climatic influence on peatland formation and lateral expansion in sub-arctic Fennoscandia: peatland formation in sub-arctic Fennoscandia. *Boreas* 39, 761–769. <https://doi.org/10.1111/j.1502-3885.2010.00168.x>.
- Weijers, J.W.H., Schouten, S., Hopmans, E.C., Geenevasen, J.A.J., David, O.R.P., Coleman, J.M., Pancost, R.D., Sinninge Damsté, J.S., 2006. Membrane lipids of mesophilic anaerobic bacteria thriving in peats have typical archaeal traits. *Environ. Microbiol.* 8, 648–657. <https://doi.org/10.1111/j.1462-2920.2005.00941.x>.
- Weijers, J.W.H., Schouten, S., van den Donker, J.C., Hopmans, E.C., Sinninge Damsté, J.S., 2007. Environmental controls on bacterial tetraether membrane lipid distribution in soils. *Geochim. Cosmochim. Acta* 71, 703–713. <https://doi.org/10.1016/j.gca.2006.10.003>.
- Williams, J.W., Shuman, B., 2008. Obtaining accurate and precise environmental reconstructions from the modern analog technique and North American surface pollen dataset. *Quat. Sci. Rev.* 27, 669–687. <https://doi.org/10.1016/j.quascirev.2008.01.004>.
- Xu, S., Zhang, Z., Jia, G., Yu, K., Lei, F., Zhu, X., 2020. Controlling factors and environmental significance of BIT and δ13C of sedimentary GDGTs from the Pearl River Estuary, China over recent decades. *Estuarine. Coast. Shelf Sci.* 233, 106534. <https://doi.org/10.1016/j.ecss.2019.106534>.
- Yao, Y., Zhao, J., Vachula, R.S., Werne, J.P., Wu, J., Song, X., Huang, Y., 2020. Correlation between the ratio of 5-methyl hexamethylated to pentamethylated branched GDGTs (HPS) and water depth reflects redox variations in stratified lakes. *Org. Geochem.* 147, 104076. <https://doi.org/10.1016/j.orggeochem.2020.104076>.
- Zell, C., Kim, J.-H., Hollander, D., Lorenzoni, L., Baker, P., Silva, C.G., Nittrouer, C., Sinninge Damsté, J.S., 2014. Sources and distributions of branched and isoprenoid tetraether lipids on the Amazon shelf and fan: implications for the use of GDGT-based proxies in marine sediments. *Geochim. Cosmochim. Acta* 139, 293–312. <https://doi.org/10.1016/j.gca.2014.04.038>.
- Zhao, B., Castañeda, I.S., Bradley, R.S., Salacup, J.M., de Wet, G.A., Daniels, W.C., Schneider, T., 2021. Development of an in situ branched GDGT calibration in Lake 578, southern Greenland. *Org. Geochem.* 152, 104168. <https://doi.org/10.1016/j.orggeochem.2020.104168>.
- Zhao, B., Russell, J.M., Tsai, V.C., Blaus, A., Parish, M.C., Liang, J., Wilk, A., Du, X., Bush, M.B., 2023. Evaluating global temperature calibrations for lacustrine branched GDGTs: seasonal variability, paleoclimate implications, and future directions. *Quat. Sci. Rev.* 310, 108124. <https://doi.org/10.1016/j.quascirev.2023.108124>.